American Mineralogist, Volume 88, pages 647–652, 2003

Biomimetic control of crystal assembly by growth in an organic hydrogel network

OLAF GRASSMANN,[1] REINHARD B. NEDER,[2] ANDREW PUTNIS,[3] AND PEER LÖBMANN[1,*]

[1]Lehrstuhl für Silicatchemie, University of Würzburg, Röntgenring 11, D-97070 Würzburg, Germany
[2]Mineralogisches Institut, University of Würzburg, Am Hubland, D-97074 Würzburg, Germany
[3]Institut für Mineralogie, University of Münster, Corrensstraße 24, D-48149 Münster, Germany

ABSTRACT

Calcite aggregates are mineralized in an organic poly-acrylamide hydrogel using a counter diffusion arrangement. The particles obtained show a characteristic pseudo-octahedral morphology, which is unexpected for calcite crystals. Scanning and transmission electron microscopy reveal a microstructure composed of individual highly aligned calcite crystallites. Although the aggregates consist of independent crystallites, the X-ray diffraction patterns suggest calcite single crystals. By analogy with some biominerals, the inorganic assembly is intergrown with an organic hydrogel network. A specific model is proposed for growth of the aggregate.

INTRODUCTION

The control of size, shape, and assembly of crystalline materials is a hallmark of biomineralization processes (Baeuerlein 2000). Most prominent examples are abalone shells (Schäffer et al. 1997), bone (Weiner et al. 1999), enamel (Fincham et al. 1999), eggshells (Fink et al. 1992), and the exoskeleton of diatoms (Kröger and Sumper 1998; Fischer et al. 1999), where minerals such as the $CaCO_3$ polymorphs calcite and aragonite, apatite, and SiO_2 are deposited in unique microstructures.

In multicellular organisms, biomineralization predominantly takes place in extracellular protein- or protein-polysaccharide networks, which are assembled in a supramolecular reaction environment (Mann 1996). Even though much work has been done on the role of these matrices in the formation of enamel, bone (Lowenstam and Weiner 1989; Traub et al. 1989) and nacre, many general aspects of size and shape control of mineralization in biological networks are not yet fully understood and are thus the subject of current research activities (Busch et al. 1999; Falini et al. 2000).

Artificial hydrogel networks, e.g., silica or poly-acrylamide, have been widely used for crystal growth experiments (Henisch 1988). For some systems a fundamental understanding of the complex interrelationship between factors such as connectivity of pores, local supersaturation, change of supersaturation and resulting crystal morphology have been established (Putnis et al. 1995). For some biomineralization products, however, crystal growth does not seem to follow generally accepted mechanisms. Calcite spines of adult sea urchin for example, show a non-crystallographic surface texture, deviating from the appearance of $CaCO_3$ grown in inorganic media (Mann 2001).

In this paper, we describe the growth of $CaCO_3$ within a poly-acrylamide hydrogel network by a counterdiffusion arrangement. The inorganic material is mineralized in an organized pseudo-octahedral assembly of rhombohedral crystallites forming a distorted single crystal. The organic matrix is partially incorporated into the oriented growing macrocrystal. Since the oriented assembly of crystalline subunits within a macromolecular matrix is a key feature of biomineralization, the study of this artificial mineralization may prove useful for a deeper understanding of biomineralization processes.

EXPERIMENTAL PROCEDURE

Synthesis of hydrogels

All chemicals except acrylamide (Fluka) were purchased from Aldrich and were used without any further purification. Demineralized water (conductivity 0.055 μS) was used as polymerization solvent. Poly-acrylamide hydrogels were prepared from acrylamide (AAm) and N,N'-methylenebis-acrylamide in a molar ratio of 29:1. The total monomer concentration of the aqueous polymerization solution was fixed at 1.4 *M*, corresponding to an overall polymer content of approximately 10 mass% within the hydrogels. The radical polymerization was initiated by ammonium-peroxodisulfate (APoxS) and N,N,N',N'-tetramethylethylene-diamine (TMEDA). The concentrations of APoxS and TMEDA were set to 1.8 and 10.1 mM respectively. After addition of the initiator, the solution was kept at 45 °C for one hour to ensure homogeneous polymerization. Gelation occurred within 6–8 minutes. The as-synthesized hydrogels were stored at ambient temperature for 48 hours to achieve complete polymerization. After aging, the hydrogels were extracted for four days in a 0.05 *M* solution of tris(hydroxymethyl)-aminomethane, which was adjusted with a 2 *M* solution of HCl to a pH of 8.35 (Tris-HCl). This ensured that components not covalently linked to the network were removed and that the pH of the pore solution was 8.35, as confirmed by pH measurement with an inserted pH electrode.

Crystallization experiments

Mineralization experiments are conducted in a double diffusion arrangement. Hydrogels with a diameter of 25 mm and

* E-mail: loebmann@silchem.uni-wuerzburg.de

0003-004X/03/0004–647$05.00

a thickness of approximately 35 mm were placed in a U-shaped tube between two aqueous solutions, 0.1 *M* $CaCl_2$ and 0.1 *M* $NaHCO_3$, respectively. To exclude the influence of a non-uniform pH throughout the gel column, the solutions were buffered with Tris-HCl to a constant pH of 8.35. In the course of diffusion the components meet in the hydrogel and precipitation of $CaCO_3$ occurs. After one week the double diffusion experiments were terminated. The hydrogel was removed from the tube and cut into 5 mm thick slices. To isolate the inorganic precipitates from the hydrogel, the slices were incubated for 24 hours in a sodium hypochlorite solution, which oxidized the organic hydrogel network. The remaining inorganic material was separated by centrifugation.

The solid phases were analyzed by powder X-ray diffraction (XRD, Stoe Stadi P), polarization microscopy (Leica DMRM), scanning electron microscopy (SEM, Hitachi S800), and thermogravimetric analysis (TGA, Setaram TAG24). To obtain further microstructural information some particles were embedded in epoxy resin (Struer Epofix) and cut with an ultramicrotome. Samples several tens of nanometers thick were examined by transmission electron microscopy (TEM, Philips CM12) and selected-area electron diffraction technique (SAED). X-ray structural analysis of individual particles was performed with a three-circle single crystal diffractometer equipped with a CCD camera (Bruker AXS, SMART APEX-detector).

RESULTS AND DISCUSSION

Biomimetic crystal assembly

Double-diffusion experiments in poly-acrylamide networks yield characteristically shaped crystalline precipitates throughout the hydrogel bodies. In contrast to Mg-bearing calcite grown in a silica gel (Fernandez-Diaz et al. 1996), the aggregate morphology does not depend on the location within the hydrogel, indicating a less pronounced effect of the local chemical environment on crystal growth. After one week, twisted "pseudo-octahedra" with diameters between 150 and 250 μm were observed (Fig. 1a). Even though $CaCO_3$ is not expected to grow with this exceptional morphology, X-ray powder diffraction experiments (XRD) of ground samples (data not shown) confirmed that the material is calcite. The pseudo-octahedral particles are composed of numerous rhombohedral crystals with diameters under 5 μm, characterized by angles of approximately 102° and 78° between edges of the rhombohedra, corresponding to the $\{10\bar{1}4\}$ faces (hexagonal axes, $c:a$ = 3.419:1). All rhombohedra are well aligned and their threefold axes are parallel to the threefold axis of the macroscopic pseudo-octahedron. Upon closer inspection of the particle surface by SEM (Fig. 1b) we observed that the dimensions of the rhombohedra cover a wide range of sizes. Comparable observations were reported for systems of self-similarity (Busch et al. 1999), which might indicate a fractal crystal growth process for the pseudo-octahedral aggregates.

Thin-cut samples of the aggregates were investigated by optical polarization microscopy. When the samples are examined with crossed polarizers, the pseudo-octahedra show a uniform birefringence (Fig. 2). Thus, the crystallographic orientation throughout the particles is nearly homogeneous, which is unexpected for assemblies composed of individual crystals. Some aggregates were cut normal to the optical axis and thus are not birefringent (see arrow in Fig. 2). These aggregates also show the trigonal morphology that is to be expected for this orientation. Compared to this, the bright interference colors of other particles results from sections parallel to the optical axis, i.e., the crystallographic **c**-axis. Consequently, the optical properties of the pseudo-octahedral aggregates show single crystal behavior.

The microstructure of the calcite aggregates was analyzed by TEM. Figure 3 shows a transmission electron micrograph of a slice cut with an ultramicrotome. Apart from artifacts due to the sample preparation, a parallel alignment of crystallites with hexagonal cross sections can be observed in the sample. The crystallite faces of the individual components are in close contact with each other. Selected-area electron diffraction patterns of adjacent crystallites show the same crystallographic

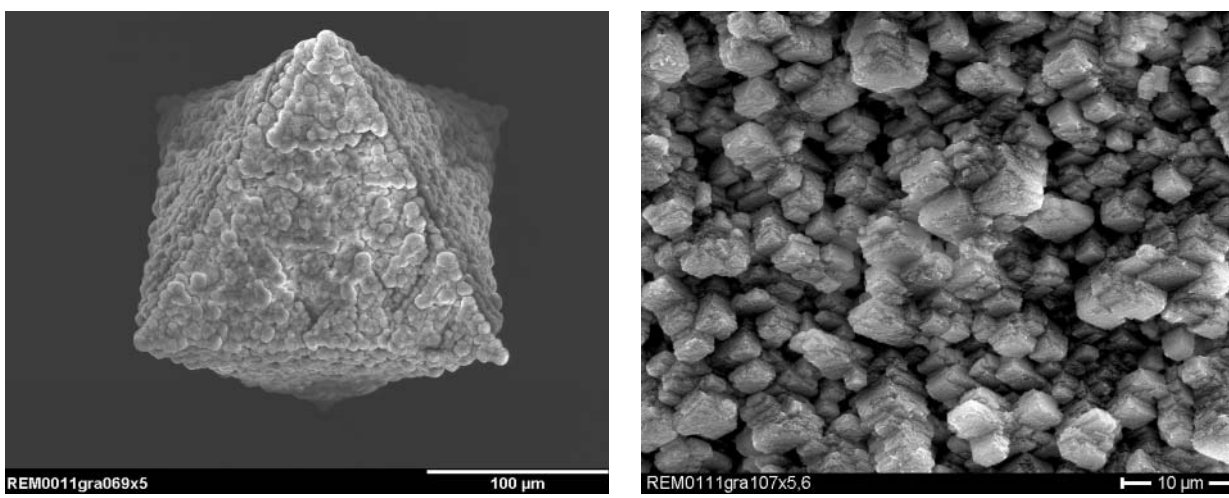

FIGURE 1. SEM-image of a aggregate with characteristic pseudo-octahedral morphology (**a**, left); surface of an aggregate with tilted rhombohedral sub-crystals and hierarchical crystal size distribution (**b**, right).

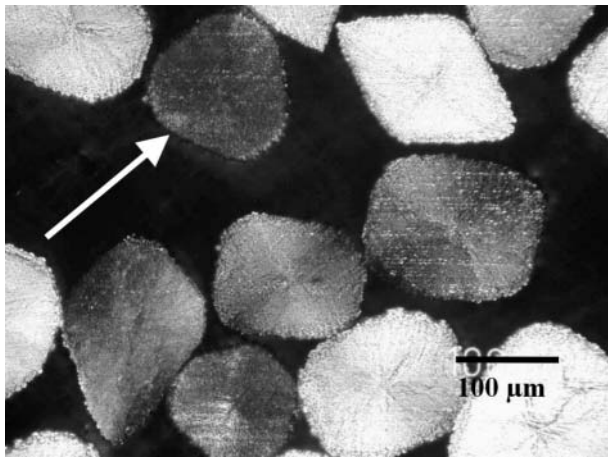

FIGURE 2. Polarization microscopic image of a cross section of poly-acrylamide-grown calcite aggregates (crossed polarizers). The dotted texture of the aggregates is due to sample preparation. The arrow indicates isotropic orientation of a calcite aggregate.

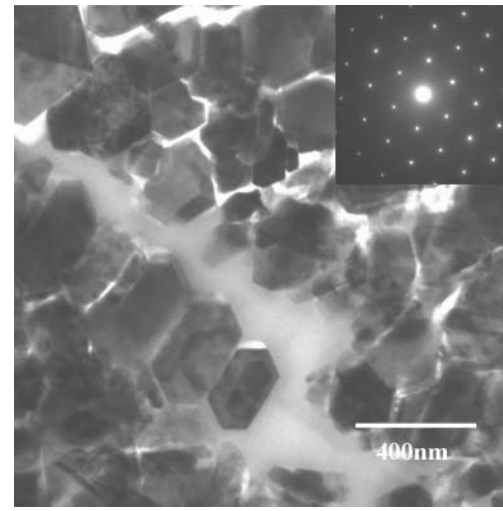

FIGURE 3. TEM image of the microstructure of a poly-acrylamide-grown aggregate showing alignment of individual crystallites. An electron diffraction pattern of an individual calcite crystallite is inserted.

orientation (see insert in Fig. 3). Apparently, self-assembling of the crystallites takes place, leading to a uniform orientation. Although the pseudo-octahedral assemblies are composed of many individual crystallites, the particles resemble a single crystal at the macro-scale. Bright areas between the crystallites may be due to incorporation of the organic poly-acrylamide matrix, although these interstices probably are accentuated in the course of thin-sectioning.

To examine the intergrowth of the crystalline calcite phase and the organic hydrogel network, some pseudo-octahedral assemblies were mechanically isolated from the hydrogels and briefly etched with sodium hypochlorite to remove organic surface contamination. Thermogravimetric analysis (TGA) and differential thermal analysis (DTA) showed that about 0.7 mass% organic hydrogel network is incorporated into the material (data not shown). As in biomineralization, where protein networks remain closely associated with the inorganic product, the pseudo-octahedral assemblies contain significant amounts of organic residues of their growth medium.

Single-crystal diffraction

The crystal structure of the pseudo-octahedra has been analyzed by single crystal X-ray diffraction. Several individual pseudo-octahedra were mounted on glass tips and placed in a three-circle single-crystal diffractometer. A typical diffraction pattern is shown in Figure 4a. Even though the diffraction spots are broad and irregularly shaped, no continuous ring-pattern was observed, as would be expected for a random assembly of crystallites. The diffraction pattern was indexed with a single orientation matrix. Due to the large mosaic spread and uneven mosaic distribution, the automatic indexing routines offered by the analysis software SMART did not provide an orientation matrix. Consequently, the orientation matrix was determined manually. Using the *d*-spacings, the innermost reflections were uniquely identified as the $\{01\bar{1}2\}$, $\{10\bar{1}4\}$, and $\{0006\}$ reflections, which were initially indexed with a dummy orientation matrix. Using this matrix, the angles between the reflections were calculated with the program DISCUS (Proffen and Neder 1997). The reflections were indexed by comparing the observed angles to calculated angles based on the known lattice constants. Subsequently, a transformation matrix from the initial dummy matrix to the correct orientation matrix was calculated. The initial orientation matrix was refined and yielded the correct lattice constants. All reflections were indexed by this orientation matrix, proving that the sample is a single crystal with a large mosaic spread.

A rocking curve together with the corresponding diffraction pattern are shown in Figure 4b. Examination of different rocking curves of the $\{10\bar{1}4\}$ reflections yielded an average mosaic spread of 3.9 ± 1.1 degrees. Interestingly, the half width of the $\{11\bar{1}0\}$ reflections is significantly smaller (1.7 ± 0.3), indicating an anisotropic mosaic spread of the single crystalline assembly. In contrast to the X-ray diffraction patterns of the pseudo-octahedral macrocrystals electron diffraction spots of individual crystallites (Fig. 3) show no broadening. Thus the broadening of the X-ray diffraction peaks is due to slight variations in the orientation of the crystallites, probably due to the incorporation of organic network material between individual crystallites.

Since the calcite assemblies are (distorted) single crystals, it is possible to determine the Miller indices of the pseudo-octahedral faces. Figure 1 shows that the particles are composed of numerous rhombohedra. As the corners of the rhombohedra, i.e., the four-body diagonals of the cleavage rhombohedron, stand roughly normal to the pseudo-octahedral faces, the Miller indices of the calcite assembly were at first deduced geometrically. The vectorial addition of the rhombohedron face normals (using the rhombohedral axes notation) resulted in the corresponding Miller indices of the pseudo-oc-

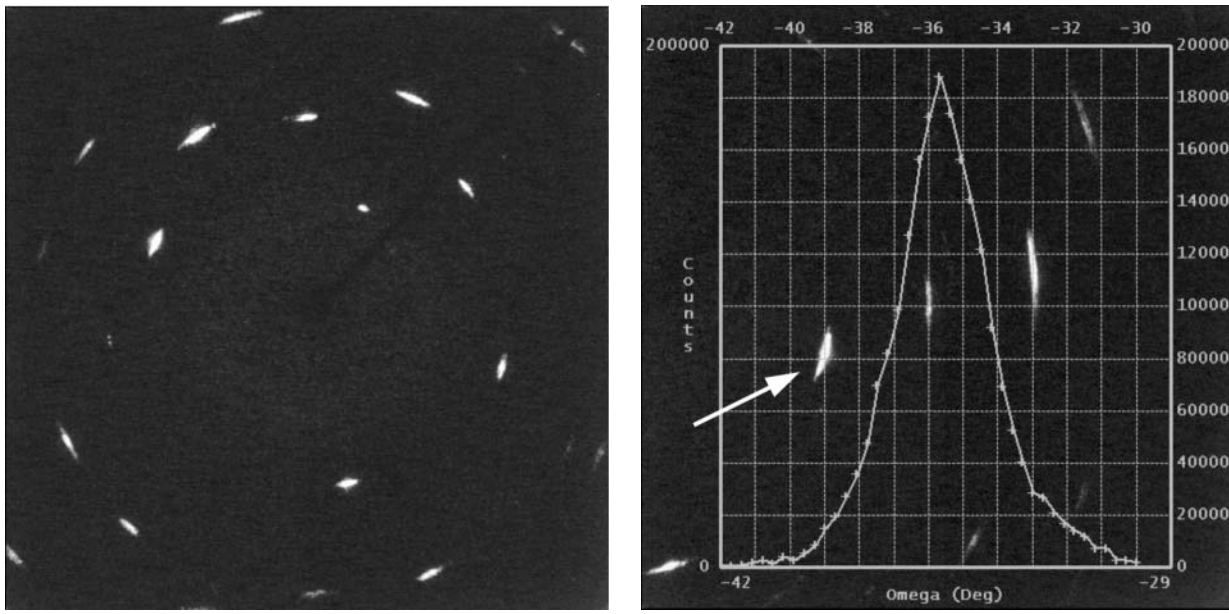

FIGURE 4. Single-crystal diffraction pattern of a poly-acrylamide grown calcite aggregate (**a**, left); rocking curve (**b**, right), the corresponding reflection is indicated by an arrow.

tahedral faces. To confirm the indices, the angles between the pseudo-octahedral faces were determined by aligning these faces parallel to the optical microscope attached to the single crystal diffractometer. In Table 1 the angles between the eight faces of the pseudo-octahedra (upper right) are compared to the theoretical interfacial angles of an ideal octahedron (lower left). It is remarkable that the measured interfacial angles correspond to the angles between the faces of the cubic octahedron. Thus, it is justifiable to call the calcite assemblies "pseudo-octahedral."

The interfacial angles corresponding to the geometrically deduced Miller indices were calculated with the program DISCUS and were compared with the optically determined angles. As the measured interfacial angles of the pseudo-octahedra deviate from the theoretical angles of the geometrically determined set of faces, the Miller indices of the pseudo-octahedra were alternatively calculated by using the refined orientation matrix. The corresponding indices of the measured interfacial angles were determined with the software SMART using the initial dummy matrix. The transformation to the refined orientation matrix yielded the correct Miller indices of the pseudo-octahedral faces: (0001) (000$\bar{1}$), (01$\bar{1}$1) (0$\bar{1}$1$\bar{1}$), (1$\bar{1}$01) ($\bar{1}$10$\bar{1}$), and ($\bar{1}$011) (10$\bar{1}\bar{1}$). By comparing the theoretical angles of these faces (Table 2: lower left) with the measured interfacial angles (Table 2: upper right), we see that the Miller indices represent the observed crystal faces.

Using the software JCRYSTAL, the theoretical crystal morphology for the calculated Miller indices could be illustrated. In fact, the crystal morphology for a set of {0001} and {01$\bar{1}$1} faces resembles an octahedron (Fig. 5a). The corresponding stereographic projection is shown in Figure 5b. The projections of the {10$\bar{1}$4} faces are also shown to clarify the orientation of the pseudo-octahedral faces in relation to the crystal faces of a calcite cleavage rhombohedron. It is obvious that the pseudo-octahedral crystal shape is in agreement with the symmetry of the calcite point group.

TABLE 1. Measured interfacial angles (°) between pseudo-octahedral faces (upper right) and angles between ideal cubic octahedral faces (lower left, italic)

Face	1	2	3	4	5	6	7	8
1	0	173	104	75	73	108	79	107
2	*180*	0	74	107	100	79	105	69
3	*109*	*71*	0	177	66	111	59	113
4	*71*	*109*	*180*	0	111	72	123	65
5	*71*	*109*	*71*	*109*	0	176	108	68
6	*109*	*71*	*109*	*71*	*180*	0	69	114
7	*71*	*109*	*71*	*109*	*109*	*71*	0	171
8	*109*	*71*	*109*	*71*	*71*	*109*	*180*	0

TABLE 2. Measured interfacial angles (°) between pseudo-octahedral faces (upper right) and angles corresponding to the Miller indices, calculated with the refined orientation matrix (lower left, italic)

h	*k*	*i*	*l*	Face	1	2	3	4	5	6	7	8
0	0	0	$\underline{1}$	1	0	173	104	75	73	108	79	107
0	$\underline{0}$	0	$\underline{1}$	2	*180*	0	74	107	100	79	105	69
0	1	$\underline{1}$	1	3	*104*	*76*	0	177	66	111	59	113
0	$\underline{1}$	1	1	4	*76*	*104*	*180*	0	111	72	123	65
$\underline{1}$	1	0	$\underline{1}$	5	*76*	*104*	*66*	*114*	0	176	108	68
$\underline{1}$	1	0	1	6	*104*	*76*	*114*	*66*	*180*	0	69	114
$\underline{1}$	0	$\underline{1}$	$\underline{1}$	7	*76*	*104*	*66*	*114*	*114*	*66*	0	171
1	0	1	1	8	*104*	*76*	*114*	*66*	*66*	*114*	*180*	0

Aggregate growth model

The morphology and assembly of the rather unusual aggregates cannot easily be explained by conventional crystal growth models. Both the microstructure and the pseudo-cubic crystal shape point to a specific aggregate growth mechanism. Classical calculations of crystal growth are based on the integration of atomic building blocks into energetically favorable sites on a growing crystal face (Kossel 1927; Stranski 1928). This pro-

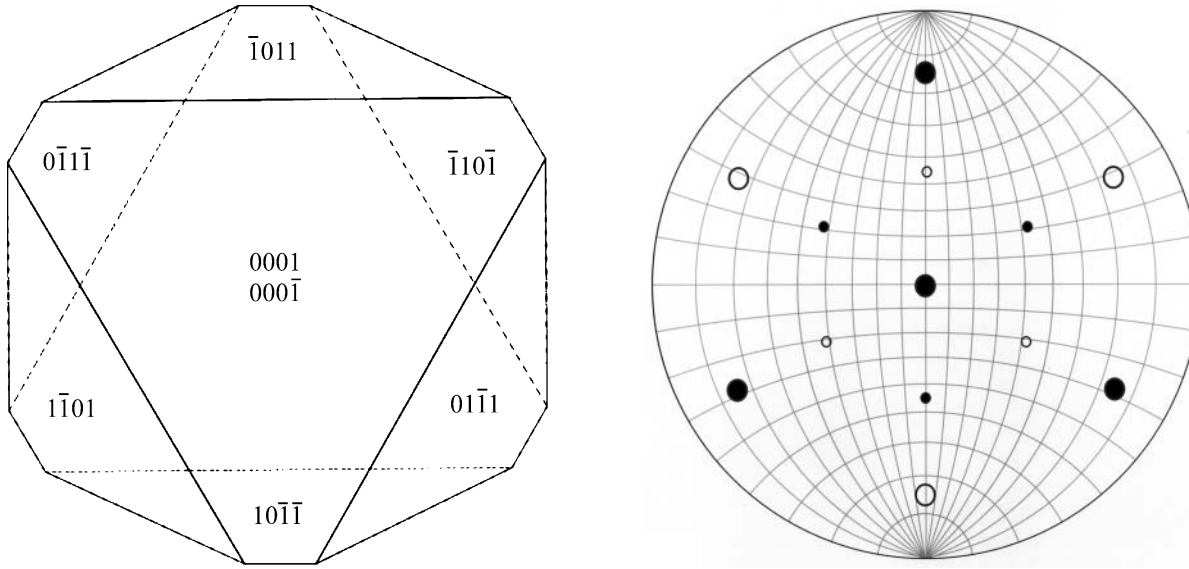

FIGURE 5. Pseudo-octahedral morphology of a combination of {0001} and {$01\bar{1}1$} forms (**a**, left); stereographic projection of {0001}, {$01\bar{1}1$} (large symbols) and {$10\bar{1}4$} faces (small symbols) (**b**, right).

cess assumes the adsorption of ions onto the crystal face and subsequent diffusion across the surface to steps and kink sites (Burton et al. 1951). The layerwise growth mechanism requires these adsorbed species to diffuse in the solution as well as on the surface of the crystal. In biomineralization, however, self-assembly of nanometer-sized particles is observed (Banfield et al. 2000). These building blocks are too big to diffuse on the surface of a growing crystal, so the growth process is rather aggregation-based, including rotation of the particles and oriented attachment of nanocrystals (Alivisatos 2000).

We assume a comparable growth mechanism for the formation of gel-grown pseudo-octahedral assemblies. Crystal growth in gel media takes place under very high supersaturations (Putnis et al. 1995). Increasing the supersaturation leads to a decrease of the activation energy for nucleation and an increase of the rate of nucleation. Consequently, the number of homogeneously nucleated clusters within the hydrogel network is large compared to crystal growth in diluted solutions. Only very few clusters reach supercritical dimensions and continue growing to macroscopic aggregates. We assume that the specific poly-acrylamide hydrogel used in our experiments contains a large supply of nanometer-sized building blocks as well as some nucleation centers. The building blocks are too large for surface diffusion on a growing nucleus. Moreover, the nanometer-sized clusters are immobilized within the covalently linked hydrogel network, so that the bulk diffusion to energetically favorable sites of the crystal is limited.

For growth of the unusual calcite aggregates, we postulate a specific mechanism of crystallization (Fig. 6): the supercritical nuclei grow due to the incorporation of ions at energetically

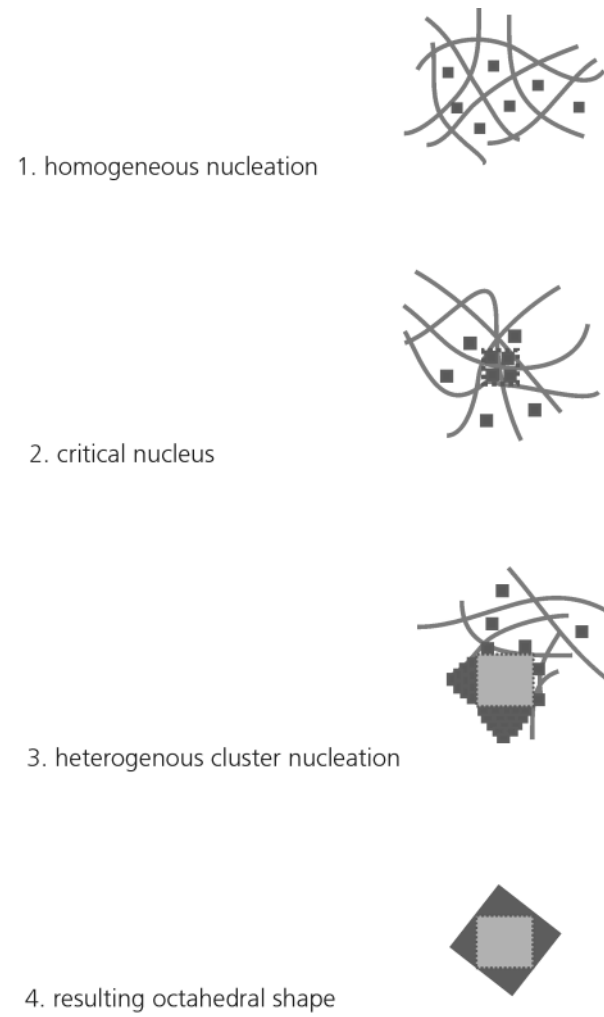

FIGURE 6. Schematic illustration of an aggregation growth process; homogeneous nucleation in the pores of poly-acrylamide (**1**); formation of a critical nucleus (**2**); oriented aggregation of preformed clusters (**3**); resulting octahedral morphology (**4**)

favorable sites, resulting in a rhombohedral arrangement. When the interface of these growing crystals comes into contact with the short-range ordered clusters, these rotate to align with the crystallographic matching face of the substrate. The cluster aggregation is driven by reduction in surface free energy that is minimized if the clusters are in contact with a crystal face rather than with edges or vertices. Thus, the growth rate of the flat faces exceeds the rate of the vertices of the rhombohedron-like supercritical nuclei. A further consumption of preformed clusters to the $\{10\bar{1}4\}$ faces in combination with crystal growth by ionic supply leads to the pseudo-octahedral shape of the resulting macroscopic aggregate.

Following general geometric considerations, a cube could only be transformed to an octahedron by the fractal attachment of cubic building blocks (Stewart 1997). Comparably, the faces of the pseudo-octahedral assemblies are composed of rhombohedra of hierarchical size distribution. Thus, we propose that simultaneously rhombohedral-shaped crystallites already attached to the surface of the supercritical nucleus continue growing while other preformed building blocks attach to the growing crystal. To grow an octahedron of macroscopic size, it is necessary that growth by ionic supply (generation of $\{10\bar{1}4\}$ faces) and attachment of building blocks (growth of pseudo-octahedra faces) are in dynamic equilibrium.

During the course of aggregate growth, the covalently linked poly-acrylamide hydrogel network is incorporated into the pseudo-octahedral assemblies, as confirmed by thermogravimetric analysis. The large mosaic spread of the single crystal X-ray diffraction pattern indicates a mismatch of the individual building blocks resulting from a non-perfect alignment during aggregate growth (Fig. 4a).

A comparable aggregation process is described for the crystallization of calcite in a silica gel at elevated pH (Dominguez Bella and Garcia-Ruiz 1986). The observed sheaf of wheat morphologies result from aggregation of rhombohedra along the **c**-axis. Although the morphology of these crystals is quite distinct from the pseudo-octahedral assemblies grown in poly-acrylamide, the aggregation of individual crystallites appears to be a general feature of crystallization at high supersaturations. The driving force of the aggregation remains ambiguous. Zeolite crystals, however, undergo spontaneous aggregation at the isoelectric point in aqueous sols (Mäurer et al. 2001) suggesting to an electrochemical effect. Whether similar electrostatic forces are essential for the described calcite aggregation process will be the subject of further investigations.

ACKNOWLEDGMENTS

This work was supported by the Deutsche Forschungsgemeinschaft (DFG) within the framework of the Schwerpunktprogramm (SPP) "Prinzipien der Biomineralisation." The authors thank G. Müller for helpful discussions and A. Dutschke for her close collaboration in the TEM study.

REFERENCES CITED

Alivisatos, A. (2000) Naturally Aligned Nanocrystals. Science, 289, 736–737.
Baeuerlein, E. (2000) Biomineralization: From Biology to Biotechnology and Medical Application. Wiley-VCH, Weinheim.
Banfield, J., Welch, S., Zhang, H., Thomsen Ebert, T., and Lee Penn, R. (2000) Aggregation-based crystal growth and microstructure development in natural iron oxyhydroxide biomineralization products. Science, 289, 751–754.
Burton, W.K., Cabrera, N., and Frank, F.C. (1951) The growth of crystals and the equilibrium structure of their surfaces. Philosophical Transactions of the Royal Society of London, 243, 299–358.
Busch, S., Dolhaine, H., DuChesne, A., Heinz, S., Hochrein, O., Laeri, F., Podebrad, O., Vietze, U., Weiland T., and Kniep, R. (1999) Biomimetic morphogenesis of fluorapatite-gelatin composites: Fractal growth, the question of intrinsic electric fields, Core-Shell assemblies, hollow spheres and reorganization of denatured collagen. European Journal of Inorganic Chemistry, 10, 1643–1653.
Dominguez Bella, S. and Garcia-Ruiz, J. (1986) Textures in induced morphology crystal aggregates of $CaCO_3$: sheaf of the wheat morphologies. Journal of Crystal Growth, 79, 236–240.
Falini, G., Fermani, S., Gazzano, M., and Ripamonti, A. (2000) Polymorphism and architectural crystal assembly of calcium carbonate in biologically inspired polymeric matrices. Journal of the Chemical Society, Dalton Transactions, 21, 3983–3987.
Fernandez-Diaz, L., Putnis, A., Prieto, M., and Putnis, C. (1996) The role of magnesium in the crystallization of calcite and aragonite in a porous medium. Journal of Sedimentary Research, 66, 482–491.
Fink, D., Caplan A., and Heuer, A. (1992) Eggshell mineralization: A case study of a bioprocessing strategy. Materials Research Society Bulletin, 10, 27.
Fincham, A., Moradian, J., and Simmer, J., (1999) The structural biology of the developing dental enamel matrix. Journal of Structural Biology, 126, 270–299.
Fischer, H., Robl, I., Sumper, M., and Kröger, N. (1999) Targeting and covalent modification of cell wall and membrane proteins heterogeneously expressed in the diatom cylindrotheca fusiformis (Bacillariophyceae). Journal of Phycology, 35, 113–120.
Henisch, H. (1988) Crystals in Gels and Liesegang Rings. Cambridge University Press, U.K.
Kossel, W. (1927) Zur Theorie des Kristallwachstums. Nachrichten von der Gesellschaft der Wissenschaften zu Göttingen, Mathematisch-Physische Klasse, 135–143.
Kröger, N. and Sumper, N. (1998) Diatom cell wall proteins and the cell biology of silica biomineralization. Protist, 149, 213–219.
Lowenstam, H. and Weiner, S. (1989) On Biomineralization. Oxford University Press, Oxford.
Mann, S. (1996) Biomimetic Materials Chemistry. VCH, Weinheim.
——— (2001) Biomineralization. Principles and Concepts in Bioinorganic Materials Chemistry. Oxford University Press.
Mäurer, T., Müller, S., and Kraushaar-Czarnetzki, B. (2001) Aggregation and peptization behavior of zeolite crystals in sols and suspensions. Industrial and Engineering Chemistry Research, 40, 2573–2579.
Proffen, T. and Neder, R. (1997) Discus: a program for diffuse scattering and defect structure-simulation. Journal of Applied Crystallography, 30, 171–175.
Putnis, A., Prieto, M., and Fernandez-Diaz, L. (1995) Fluid supersaturation and crystallization in porous media. Geological Magazine, 132, 1–13.
Schäffer, T., Ionescu-Zanetti, C., Proksch, R., Fritz, M., Walters, D., Almqvist, N., Zaremba, C., Belcher, A., Smith, B., Stucky, G., Morse, D., and Hansma, P. (1997) Does abalone nacre form by heteroepitaxial nucleation or by growth through mineral bridges? Chemistry of Materials, 9, 1731–1740.
Stewart, I. (1997) Die Skulpturen von Alan St. George. Spektrum der Wissenschaft, 10, 12–16.
Stranski, I.N. (1928) The theory of crystal growth. Zeitschrift für Physikalische Chemie, 136, 259–278.
Traub, W., Arad, T., and Weiner, S. (1989) Three-dimensional ordered distribution of crystals in turkey tendon collagen fibers. Proceedings of the National Academy of Sciences of the U.S.A., 86, 9822–9826.
Weiner, S., Traub, W., and Wagner, H. (1999) Lamellar bone: Structure-function relations. Journal of Structural Biology, 126, 241–255.

MANUSCRIPT RECEIVED MAY 23, 2002
MANUSCRIPT ACCEPTED NOVEMBER 4, 2002
MANUSCRIPT HANDLED BY KATRINA EDWARDS